Published in final edited form as:

Mol Cancer Ther. 2015 April ; 14(4): 899–908. doi:10.1158/1535-7163.MCT-14-0775.

Magnetic resonance spectroscopy for detection of choline kinase inhibition in the treatment of brain tumors

Manoj Kumar[1,†], **Sean P. Arlauckas**[1,†], **Sona Saksena**[1], **Gaurav Verma**[1], **Ranjit Ittyerah**[1], **Stephen Pickup**[1], **Anatoliy V. Popov**[1], **Edward J. Delikatny**[1], and **Harish Poptani**[1,2,*]

[1]Department of Radiology, Perelman School of Medicine at the University of Pennsylvania, Philadelphia, PA 19104

[2]Department of Cellular and Molecular Physiology, Institute of Regenerative Medicine, University of Liverpool, Crown Street, Liverpool L69 3BX, United Kingdom

Abstract

Abnormal choline metabolism is a hallmark of cancer and is associated with oncogenesis and tumor progression. Increased choline is consistently observed in both pre-clinical tumor models and in human brain tumors by proton magnetic resonance spectroscopy (MRS). Thus, inhibition of choline metabolism using specific choline kinase inhibitors such as MN58b may be a promising new strategy for treatment of brain tumors. We demonstrate the efficacy of MN58b in suppressing phosphocholine production in three brain tumor cell lines. *In vivo* MRS studies of rats with intracranial F98-derived brain tumors showed a significant decrease in tumor total choline concentration after treatment with MN58b. High resolution MRS of tissue extracts confirmed that this decrease was due to a significant reduction in phosphocholine. Concomitantly, a significant increase in poly-unsaturated lipid resonances was also observed in treated tumors, indicating apoptotic cell death. Magnetic resonance imaging (MRI) based volume measurements demonstrated a significant growth arrest in the MN58b-treated tumors in comparison to saline-treated controls. Histologically, MN58b-treated tumors showed decreased cell density, as well as increased apoptotic cells. These results suggest that inhibition of choline kinase can be used as an adjuvant to chemotherapy in the treatment of brain tumors and that decreases in total choline observed by MRS can be used as an effective phamacodynamic biomarker of treatment response.

Keywords

Animal model; Brain tumor; Choline kinase; Glioblastoma; Magnetic resonance spectroscopy; MN58b; Total choline

[*]**Address correspondence to:** Harish Poptani, PhD, Professor and Chair of the Pre-clinical imaging center, Department of Cellular and Molecular Physiology, Institute of Regenerative Medicine, University of Liverpool, Crown Street, Liverpool L69 3BX, United Kingdom, Ph: +44-151-794 5444, harish.poptani@liverpool.ac.uk.

[†]M Kumar and SP Arlauckas contributed equally to this work

The authors declare no conflicts of interest.

INTRODUCTION

Glioblastoma (GBM), the most common primary brain tumor in adults, is an aggressive and locally invasive tumor. Despite advances in surgery, radiation, and chemotherapy, overall survival of patients affected by GBM has only marginally increased from 6-14 months post-diagnosis in recent decades (1). This may partly be due to a lack of effective therapeutic options and limited availability of robust and sensitive methods to assess therapeutic response. As survival with GBM is short, it is critical to determine the efficacy of therapy early on in treatment. An increased understanding of the molecular mechanisms underlying oncogenesis has led contemporary drug discovery programs to be aimed predominantly at signal transduction pathways and molecules that drive cancer initiation and progression (2). Elevated choline kinase (ChoK) activity has been associated with enhanced synthesis of phosphocholine (PC) in many cancer cell types and has been proposed as a potential target for anticancer therapy (3). ChoK catalyzes the phosphorylation of choline, consuming ATP in the presence of Mg^{2+}, yielding PC in a process mostly independent of the rate of net phosphatidylcholine biosynthesis (4-6). Several agents such as growth factors, chemical carcinogens and *ras* oncogenic transfection induce ChoK activation in malignant cells, leading to an accumulation of PC (5).

A novel molecular therapeutic strategy focused on ChoK inhibition has recently been developed, resulting in the discovery of a group of compounds with inhibitory activity against ChoK (5, 7-9). The inhibition of ChoK using small molecule inhibitors such as MN58b (5, 8) appears to be a promising new treatment strategy against solid tumors. MN58b is an anticancer drug that exhibits selective inhibition of ChoK activity resulting in attenuated PC levels, reduced proliferation of cancer cells *in vitro*, and growth delay of human tumor xenografts (5, 8, 10-13).

There is a strong need to obtain precise surrogate biomarkers to effectively evaluate therapeutic response in GBM. ^{1}H MRS provides a novel way of non-invasively measuring changes in choline-containing tumor metabolites to serve as a pharamcodynamic biomarker of ChoK inhibition and therapeutic response. Al-Saffar *et al*. (5) have reported the efficacy of MN58b on subcutaneously implanted colon and breast cancer models, however, we are unaware of any *in vivo* MRS studies of brain tumor response to ChoK inhibition. Thus, the goal of the present study was to monitor changes in choline-containing metabolites in an intracranial model of rat glioma in response to treatment with the ChoK inhibitor, MN58b.

MATERIALS AND METHODS

Cell lines and culture

To assess the toxicity and efficacy of MN58b on growth inhibition of gliomas, we chose three rat brain tumor cell lines F98, 9L and 9L over-expressing EGFRviii (14). The F98, 9L and 9L-EGFRviii glioma cell lines were maintained as adherent monolayers cultured in Dulbecco's Modified Eagle's Medium (DMEM, Sigma-Aldrich, St Louis, MO) supplemented with 10% fetal bovine serum (HyClone, Mississauga, Canada), 1% 4-(2-hydroxyethyl)-1-piperazineethanesulfonic acid (HEPES) buffer (Invitrogen; Carlsbad, CA), 200 U/mL penicillin and 200 mg/mL streptomycin sulfate at 37°C in 5% CO_2 in air. Cells

were maintained in exponential growth phase by routine passage twice weekly at 3×10^5 cells per T75 flask. 9L and F98 cell cultures were tested upon receipt from the lab of Dr. J. Biaglow (Department of Radiation Oncology at the University of Pennsylvania) in 1999 using the Rat Antibody Production (RAP) Test performed by Charles River Laboratories (Wilmington, MA) and re-screened in 2005 using IMPACT III PCR profiling performed by RADIL (Columbia, MO). Cell lines were used within 6 months of reconstitution and tested bi-monthly for mycoplasma. The 9L-EGFRviii cell line was cloned from the 9L cells in the laboratory of Dr. Donald M O'Rourke, Department of Neurosurgery, University of Pennsylvania. We obtain 9L-EGFRviii cell lines from Dr. Donald M O'Rourke in 2010. No additional characterization has been performed on this cell line.

3-(4,5-Dimethylthiazol-2-yl)-2,5-diphenyltetrazolium bromide; thiazolyl blue (MTT) Assay

The F98, 9L and 9L-EGFRviii rat glioma cell lines were plated in quadruplicate in 96-well plates at 7.5×10^4 cells/well and incubated overnight. Culture medium was replaced with media containing varying concentrations of MN58b. After 24 h, 20 μL of 5 mg/mL MTT (Sigma-Aldrich, St Louis, MO) in sterile PBS was added and the cells were incubated for 2 h. The media/MTT mixture was removed and replaced with 150 μL dimethyl sulfoxide (DMSO, Fisher Scientific, Fair Lawn, NJ), shaken, and the absorbance read at 550 nm using a Spectra Max M5 plate reader (Molecular Devices, Sunnyvale, CA). Background signal was read as absorbance at 690 nm and subtracted from each sample.

ChoK Activity Assay

For each cell line (F98, 9L and 9L-EGFRviii), 5×10^5 cells/well were seeded in a 6-well plate and incubated for 24 h at 37°C. The exponentially growing cells were pulsed for 1 h with 0.5 μCi/mL of [methyl-^{14}C]-choline (Perkin Elmer, Shelton, CT) per well at 37°C followed by the addition of varying concentrations of MN58b, which was synthesized in house as previously described (13). After 2 h treatment, the medium was removed and cells were washed twice with ice-cold PBS and fixed in 16% ice-cold trichloroacetic acid (Fisher Scientific, Fair Lawn, NJ). ChoK inhibition was probed at 2 h because this time point has been found previously to be a time prior to significant loss in cell viability, thus providing a more accurate measurement of ChoK activity (13). Each sample was washed 3x in diethyl ether, lyophilized, and resuspended in water for thin layer chromatography (TLC) separation using a solvent system of NaCl/CH_3OH/NH_4OH; 50:70:0.5. The TLC plates were analyzed by autoradiography using a Fujifilm FLA-7000 (Tokyo, Japan) to detect radioactivity.

Perchloric acid (PCA) extracts of F98 tumor cells

F98 cells were seeded (1×10^5/mL, 150 cm^2 flasks) and incubated overnight, media was aspirated and replaced with fresh media containing 0, 10, and 20 μM MN58b. After 24 h MN58b treatment, cells were trypsinized, washed and an aliquot was removed for viability counts. The remaining cells were pelleted and homogenized in 3 vol of 6% PCA, transferred into an Eppendorf tube and centrifuged (13,000 rpm, 30 min, 4°C), neutralized with 3 M potassium hydroxide (KOH, Sigma-Aldrich, St Louis, MO) and the neutralized samples were lyophilized for 24 h.

High resolution NMR spectroscopy of tumor cell PCA extracts

Lyophilized samples were resuspended in 500 μL of deuterium oxide (D_2O, Sigma-Aldrich, St Louis, MO) including 0.5 mmol 3-(trimethylsilyl) 3,3,3,3-tetradeuteropropionic acid (TSP, Sigma-Aldrich, St Louis, MO), which was used as an internal concentration and chemical shift reference. The pD of the solution was adjusted to 7.0 using deuterium chloride (DCl, Sigma-Aldrich, St Louis, MO) or potassium deuteroxide (KOD, Sigma-Aldrich, St Louis, MO) solutions using a standard pH meter and calibrated to actual pH by adding 0.41 to the measured pH (15). High resolution NMR spectroscopy was performed at 30°C using an 11.7 T, 55-mm (inner diameter) vertical bore spectrophotometer (Bruker, Billerica, MA). The sample was first transferred to a clean, dry 5-mm thin-walled NMR tube (Wilmad-LabGlass, NJ). Fully relaxed, one-dimensional proton spectra were acquired using a pulse-acquire sequence with the following parameters: 90° pulse, TR=10.73 s, SW=6,000 Hz, NP=32 K and number of averages=64, with scan time=11 min 28 sec per sample. Acquired spectroscopic data were transferred offline for further post-processing and analysis.

Animal model and tumor cell implantation

An allogeneic rat animal model was chosen to better understand the complexities of this disease in an immune-competent rat model (16). Studies have pointed to F98 orthotropic GBM models as one of the most realistic and cost-effective simulations of the human disease due to its low immunogenicity, accurate histological representation of growth and infiltration, and refractory response to clinically-relevant therapies (17). All animal studies were approved by the Institutional Animal Care and Use Committee of the University of Pennsylvania. Six week old syngeneic female Fisher F344/NCr (120-150 gm weight) rats (n=13) were purchased from the National Cancer Institute and housed in a temperature controlled animal facility with a 12 h light-dark cycle. General anesthesia was induced by intraperitoneal injection of ketamine/xylazine (80/8.0 mg/kg). The animal was placed on a stereotactic frame. A small burr hole was made 3-mm lateral and 3-mm posterior to the bregma and 2-mm deep into the right cerebral hemisphere using a drill bit. F98 tumor cells (5×10^4) in a 10 μl suspension in PBS were inoculated over a 5-min period with a Hamilton syringe and a 30-gauge needle using a stereotactic apparatus. After injection of the cell suspension, the needle was withdrawn slowly and the wound was closed by suturing the skin. Animals were monitored periodically for 2 weeks after which baseline *in vivo* MRS experiments were performed.

In vivo MRI

Animal preparation for MRI scan—Animals were anesthetized with 3% isoflurane in oxygen and mounted on an animal holding cradle. The animal's head was secured with a nose cone in an in-house developed restraining device to minimize motion-induced artifacts. Subdural EKG needle electrodes were placed in the forelimbs and a respiration pillow was placed on the dorsal side of the body. A thermister was inserted into the rectum to monitor body temperature. EKG electrodes, respiratory pillow and thermister were connected to a small animal monitoring device (SA Instruments, NY, USA) to record vital signs including the electrocardiogram, respiration and core body temperature during the scan. The cradle

with the animal in position was then inserted inside a 35-mm inner diameter transmit-receive quadrature volume coil (M2M Imaging, Cleveland, OH, USA) and the coil was placed in the center of the magnet. During the scan, anesthesia was maintained using 1-1.5% isoflurane and the animal body temperature was regulated at 37±1°C by blowing warm air into the magnet bore via a hose connected to a thermostatically controlled warm air device (SA Instruments, NY, USA).

***In vivo* single voxel spectroscopy—**Anatomical images and spectroscopy data were acquired from the brains of 6 normal and 13 intracranial tumor bearing rats for baseline measurements. The *in vivo* MRS study was repeated on tumor bearing animals after 5 days of MN58b (n=10) or saline (n=3) injection to evaluate treatment response. *In vivo* studies were performed on a 9.4 T horizontal bore magnet equipped with 40 G/cm gradients interfaced to an Agilent Direct-Drive console (Agilent, Palo Alto, CA, USA) operating vnmrj 2.3.C software. Multi-slice spin echo and T_2-weighted anatomical images were acquired to localize the tumor and to plan the MRS voxel. A single voxel with dimensions of 3×3×3 mm^3 was placed within the tumor and a spectrum was acquired using a PRESS sequence with the following parameters: TR=3000 ms, TE_1=12.68 ms and TE_2=10.01 ms, number of averages=128, complex points=4096 and spectral width=4000 Hz resulting in an acquisition time of 6 min 24 sec. Water suppression was performed using the variable power and optimized relaxation delays (VAPOR) technique (18). An unsuppressed water spectrum was also acquired (with 8 averages) to serve as a reference for calculation of metabolite concentrations.

Treatment of tumor bearing animals with MN58b—After acquiring baseline *in vivo* MRS, 10 tumor bearing animals were treated with MN58b at 2 mg/kg/day i.p. for 5-days. A separate cohort of tumor bearing animals (n=3) were treated with an i.p. injection of 1 mL saline daily for 5-days. *In vivo* MRS experiments were repeated as described above to evaluate the effect of MN58b treatment on tumor metabolism. Two animals died during the MN58b treatment resulting in post-MN58b data from only 8 animals. The death of these animals was most likely due to the tumor burden, as no overt indications of toxicity were noted as a result of MN58b: loss of weight, change in grooming or social habits, fur ruffling, or change in eye color.

The tumor bearing animals were anesthetized with an overdose of ketamine/xylazine after the completion of the final *in vivo* ^{1}H MRS study. Following lack of deep tendon responses, the head was decapitated and the brain was removed from the skull. Tumor tissue and contralateral normal brain tissue were harvested from each animal under aseptic conditions in a laminar hood. A portion of the harvested tissue was immediately placed in a pre-weighed cryovial and flash frozen by dipping into liquid nitrogen. The frozen specimens were stored at −70 °C.

PCA extracts and high-resolution NMR studies on tumor tissue—PCA extractions and high-resolution NMR studies were performed on tissue samples from contralateral normal brain, saline and MN58b-treated tumor tissue on a 500 MHz vertical bore NMR scanner (Bruker, Billerica, MA) using the same experimental protocol as described for cell extracts.

Histopathology—A set of tissue samples was randomly selected from the saline and MN58b-treated group for histopathological study. These samples were fixed in 10% neutral buffered formalin for 24 h and were fixed and dehydrated in ethanol, cleared in xylene, and embedded in paraffin blocks, which were cooled before sectioning. Consecutive 3-micron thick serial sections were cut and stained with Hematoxylin and Eosin (H&E) or with an antibody against Caspase-3 using methods previously described (19). Saline and MN58b-treated tumor sections were examined for necrosis, hemorrhage and cell density using H&E, and apoptosis using Caspase-3 immunohistochemistry. H&E and Caspase-3 stained slides were scanned at 20 and 40 X magnifications using the Aperio Scan Scope OS (Aperio Technology, Vista, CA).

Data quantification—High-resolution NMR data from cells and tumor tissue extracts were analyzed using MestReNova (Mestrelab Research, Santiago de Compostela, Spain) to assess changes in PC and GPC levels due to MN58b treatment. Metabolite peaks were identified on the basis of their chemical shifts (20). The following choline-containing metabolites were identified from their N-trimethyl ($^{+}N(CH_3)_3$) resonances: Cho 3.20 ppm (singlet); PC, 3.22 ppm (singlet); and GPC, 3.23 ppm (singlet) referenced to the internal standard TSP at 0.0 ppm after baseline correction. Metabolite concentrations were calculated from peak heights in ^{1}H-MR spectra. The signal area in the proton spectrum is proportional to the concentration and the number of protons contributing to the signal. Because the spectra were fully relaxed and the line widths of all peaks were the same, absolute signal intensities can be determined from the peak heights by direct reference to TSP. The metabolite concentrations were calculated and corrected for the number of cells in the NMR experiment using the following formula: [(metabolite peak height /number of protons) /(TSP peak height /number of TSP protons)] × (TSP concentration /number of cells). The resonances at 3.2 ppm from the choline-containing metabolites are all composed of 9 protons, as is the 0.0 ppm resonance of TSP. The concentration of TSP was 1.93 μM and the number of cells for each experiment was in the range of 1.0-7.4×10^{7} cells. For tissue extracts, we calculated the metabolite concentration per wet-weight of the tissue, which ranged from 27.9-140 mg.

In vivo single voxel ^{1}H MRS data from normal brain, saline and MN58b-treated tumors were processed and analyzed using LC-model software (21). A least-squares algorithm (Gaussian-Lorentzian) was used to optimize the fit after individual iteration and the quality of the final fit was determined in terms of the Cramer-Rao lower bound (CRLB), a measure of the variance in the error. Only metabolites with less than 20% CRLB were considered and included in the final data analysis. A separate basis set was used to analyze the polyunsaturated lipid resonance at 2.8 ppm. Due to the complexity of overlapping lipid and lactate peak contributions at 1.3 ppm, LC model was not ideal for fitting the composite Lip+Lac resonance. Thus, we used the MestReNova program as described above to quantify the 1.3 ppm Lip+Lac peak.

To assess the effect of MN58b on tumor growth, tumor volumes were measured using T_2-weighted images acquired at baseline and after 5-days of MN58b treatment. In-house custom software developed in the IDL programming environment (ITT Visual Information Solutions, Boulder, CO, USA) was used to convert raw image data into an “analyze” file

format. The analyze files were read into MRIcro (1.39 version, McCausland Center for Brain Imaging, Columbia, SC, USA) and the ROI tool used to draw whole tumor ROIs on multiple slices covering the tumor. The final volume was calculated as the sum of pixels from all the ROIs multiplied by the section thickness.

Image Scope viewing software and nuclear staining algorithm V.9 (version 9; Aperio Technologies, Inc.) were applied to quantify nuclear density from Hematoxylin and Caspase-3 positive nuclei from Caspase-3 immunohistochemistry. Algorithm parameters were set to achieve concordance with manual scoring on a number of high-power fields, including intensity thresholds for positivity and parameters that control cell segmentation using the nuclear algorithm (22). Regions of tissue necrosis and staining artifacts were manually excluded. The algorithms calculate the percentage of weak (1+), medium (2+), and strong (3+) positive cells. The strong (3+) positive staining numbers were used to assess differences between saline and MN58b-treated tumors.

Statistical analysis

Statistical analysis of the *in vitro* and *in vivo* ^{1}H MRS data was conducted using a Student's unpaired t-test to evaluate the differences in metabolite concentration in response to MN58b treatment. A p-value of ≤0.05 was considered to be statistically significant. All error bars shown in the figures represent mean±SEM values. All statistical analysis was conducted using SPSS 16.0 (SPSS, Inc., Chicago, IL, USA).

RESULTS

MN58b was screened for its ability to inhibit the viability of a panel of brain tumor cell lines using the MTT assay. MN58b treatment significantly reduced the viability of the F98, 9L and 9L-EGFRviii cells in a dose dependent manner, with GI_{50}s of 19.80±2.80 μM, 8.60±3.00 μM and 46.85±2.30 μM, respectively (Fig. 1). The phosphorylation of ^{14}C-labeled Cho (R_f =0.07) was measured using TLC and autoradiography. ^{14}C-PC (R_f =0.14) production in the F98, 9L, and 9L-EGFRviii cells was quantified, plotted, and fitted to determine IC_{50}s of 2.63±0.65 μM, 1.84±0.53 μM, and 1.85±0.33 μM, respectively (Fig. 2A and 2B). No statistical difference in ChoK inhibition was found between these groups. Since ^{14}C-radiotracing demonstrated similar treatment response from all three cell lines, we chose F98 cells for *in vivo* studies because they most closely resemble human GBM (14, 15). The 9L is a gliosarcoma and does not exhibit the necrotic areas seen in GBM (16). 9L-EGFRviii is similar to a GBM but is not as well characterized compared to the F98 tumor model.

Cellular extracts prepared from F98 cells treated with 0, 10 or 20 μM MN58b were analyzed by NMR to determine changes in PC and GPC levels (Fig. 3A). Analysis of the choline-containing peaks showed lower PC levels in response to MN58b compared to saline-treated cells (Fig. 3B). We observed significantly reduced PC concentration in cells treated with both 10 μM MN58b (5.85±0.70 nmoles/10^7 cells) and 20 μM MN58b (6.84±3.51 nmoles/10^7 cells, p=0.049) compared to saline-treated cells (18.85±2.39 nmoles/10^7 cells, p=0.004). We also observed higher GPC concentration in cells after 10 μM MN58b treatment (6.64±2.42 nmoles/10^7 cells, p=0.911) and a further increase after 20 μM

(11.95±7.50 nmoles/10^7 cells, p=0.532) MN58b compared to saline-treated cells (6.27±1.94 nmoles/10^7 cells) but this difference was not statistically significant (Fig. 3B). Inhibition of the anabolic pathway of choline metabolism has been reported to increase GPC at the expense of PC (23). The PC/GPC ratio was thus calculated for each treatment group, and both 10 μM (0.88±0.39, p=0.012), and 20 μM MN58b (0.57±0.08, p=0.007) cells demonstrated significantly lower PC/GPC ratio as compared to saline-treated cells (3.01±0.61) (Fig. 3C).

In vivo MR spectra (Fig. 4A) were obtained for each tumor before and after saline or MN58b treatment. MN58b led to a significant growth arrest of F98 tumors as treated tumors only grew by 77±11% in comparison to saline-treated tumors, which grew by 160±31% (p=0.015) during the 5-day treatment period (Fig. 4B). The tCho concentration (1.08±0.38 mM) after MN58b treatment was significantly lower than tCho from the brains of rats used as normal controls (1.68±0.23 mM, p=0.032), baseline values for the untreated tumor (1.95±0.75 mM, p=0.005) as well as saline-treated tumors (1.92±0.24 mM, p=0.010) (Fig. 4A and 4C). When the data from individual animals were compared before and after MN58b treatment, a 44% reduction in tCho level was observed in MN58b treated animals compared to baseline values.

We observed significantly increased Lip+Lac concentration in MN58b-treated tumors (8.79±4.04 arbitrary units (AU)) compared to normal control brain (0.87±0.67 AU, p=0.002) as well as baseline tumor values (7.58±3.29 AU, p=0.048) (Fig 4D). There was no significant difference in the Lip+Lac concentration between MN58b-treated tumors and saline-treated tumor (11.87±3.59 AU, p=0.341) (Fig 4D). However, we observed an increase in the polyunsaturated fatty acyl chain resonance at 2.8 ppm after MN58b treatment (1.37±0.46 AU, p=0.018), baseline (0.51±0.42 AU, p=0.007) and saline treated (0.52±0.02 AU, p=0.010) compared to control brain (0.03±0.06, AU), respectively (Fig. 4A and 4E).

Similar to the results observed from F98 cells treated with MN58b, the *ex vivo* high resolution NMR data from tissue extracts also demonstrated changes in PC and GPC values in MN58b-treated tumors (Fig. 5A). Significantly lower PC levels were observed in MN58b-treated tumors (0.33±0.06 nmoles/mg, p=0.019) compared to saline-treated tumors (0.59±0.06 nmoles/mg). The saline-treated tumor demonstrated significantly higher PC (p=0.030) than normal brain (0.30±0.09 nmoles/mg). Significantly higher GPC was also observed in MN58b-treated tumors (0.44±0.05 nmoles/mg, p=0.009) compared to normal brain (0.23±0.05 nmoles/mg). The GPC in saline-treated tumors (0.40±0.03 nmoles/mg, p=0.015) was significantly higher than contralateral normal brain. However, the GPC concentration between saline-treated and MN58b-treated tumor was not significantly different (p=0.593). When the PC/GPC ratios were computed, a significantly lower PC/GPC ratio was observed in MN58b-treated (0.76±0.09 p=0.05) than saline-treated tumors (1.49±0.25) (Fig. 5B). However, there was no significant difference in the PC/GPC ratio between MN58b-treated (p=0.124) and normal brain (1.41±0.35) (Fig. 5C).

Immunohistological staining and quantitation was performed on a sample of saline and MN58b-treated tumors. Quantitative analysis of Hematoxylin staining, demonstrated a 16% reduction in the total number of tumor cells in MN58b-treated (1.20×10^4 cells/mm^2)

compared to saline-treated tumor (1.42×10^4 cells/mm^2, Fig. 6A-D). MN58b treatment was also associated with increased staining of Caspase-3 indicative of apoptosis (Fig. 6E-H). A 3.0 fold increase in Caspase-3 positive cells was observed in MN58b-treated (4.3% positive cells) compared to saline-treated tumor tissue (1.4% positive cells).

DISCUSSION

In this paper, the effect of the choline kinase inhibitor MN58b on choline metabolism was examined in a glioma model and a significant decrease in tCho was observed resulting from decreased levels of PC. Elevated ChoK activity in tumor cells and increased tCho levels in cells and untreated tumors suggest that increased tCho in tumors is primarily driven by elevated ChoK. The significant decrease in cellular ChoK activity after treatment with MN58b indicates that inhibition of ChoK may be an effective adjuvant in the treatment of gliomas. MRI and MRS studies of MN58b-treated orthotopic glioma tumors demonstrated significant tumor growth inhibition and reduction in tCho levels. These findings were corroborated with the histological finding of elevated apoptotic cells within MN58b-treated tumors, indicating the efficacy of MN58b as a potential therapeutic agent in the treatment of gliomas.

Over-expression and increased ChoK activity resulting in production of PC has been detected in several human tumor derived cancer cell lines and tissue biopsies including lung, colon and prostate (9-12, 24, 25). Decreased tumor tCho is usually associated with a positive response to conventional chemotherapy in cancer and suggests a role for choline compounds as potential biomarkers to assess treatment response (26). Recent studies have explored the possibility of altering the expression or activity of enzymes involved in choline metabolism as a novel therapeutic target for cancer treatment (11, 27). Inhibition of ChoK is regarded as an attractive cancer treatment strategy (28) and changes in tCho due to ChoK activity as detected by MRS can be used as a non-invasive pharmacodynamic marker of therapeutic response. MRS is an efficient technique for discrimination between brain lesions and for following treatment response (29, 30). It was not known, however, whether gliomas respond to ChoK inhibition therapy and whether MRS is capable of validating tCho as a surrogate marker of treatment response.

We studied three different glioma cell lines *in vitro* and observed their sensitivity to MN58b via MTT and ChoK assays. We observed the phosphorylation of ^{14}C-labeled choline using a TLC-based ChoK assay and found inhibition of ChoK activity in a dose dependent manner. While MN58b inhibited ^{14}C-PC production with similar potency in each of the three cell lines, the EGFRviii mutation imparted some resistance in terms of viability compared to wild-type 9L cells, which express very little EGFR. The observation of decreased ChoK activity and increased cellular toxicity in all three cell lines led us to explore ChoK inhibition *in vivo* in a rat model of brain cancer.

Higher choline levels may be suggestive of increased malignant potential (23), increased membrane turnover (31) or activation of oncogenic signaling (32). The tCho signal is commonly increased in malignant gliomas and is also associated with processes that either promote cellular proliferation or induce cell death that can be observed as changes in the

tCho peak in MRS (29). In cell extracts using high resolution ^{1}H NMR, we observed a decrease in PC and non-significant increase in GPC in response to MN58b treatment, showing the effectiveness of ChoK inhibition on choline metabolite levels. *In vivo* a significant MN58b-induced decrease in tCho was observed with ^{1}H MRS indicating inhibition of ChoK (Fig. 4A and B). MN58b treatment caused significant reduction of the PC/GPC ratio in both cellular and tumor tissue extracts, which is consistent with previously reported results. The decrease in the PC/GPC ratio was found using NMR of *ex vivo* tumor extracts to be caused primarily by a net decrease in PC levels, as previously established (5, 7, 8).

The *in vivo* data followed the same general trend as observed with *ex vivo* extracts: MN58b caused a decrease in tCho *in vivo* compared to saline treatment that was paralleled by a decrease in PC and in PC/GPC ratio in extracts. Although tCho was not significantly different in normal brain vs baseline tumor spectra *in vivo*, both PC and GPC were elevated in the extract spectra of tumors relative to contralateral tissue. Interestingly the contralateral PC/GPC ratio was also not significantly different from saline-treated tumor extracts even though their absolute levels were much lower. This variability was higher *in vivo* possibly due to heterogeneity of the tumor sampled with single voxel MRS and the relatively broad spectral line width. In addition, gliomas are often histopathologically heterogeneous and have components of varying grades of malignancy and necrosis within the tumor. A decrease in tCho and lactate, as well as an increase in lipid, would be expected in necrotic tumor tissue.

^{1}H MRS is highly sensitive to alterations in the unsaturated state of lipid acyl chains. Increased fatty acyl chain resonances in MR-visible lipids have been correlated with malignancy and necrosis in human brain tumors (33-35) and an increase in polyunsaturated fatty acids (PUFA) (36, 37), along with a decrease in lactate (38, 39), is typically observed in tumors after treatment. We observed an increase in the 1.3 ppm resonance in both untreated and treated tumors compared to baseline but increased PUFA resonance at 2.8 ppm was observed only in treated tumors. The increased PUFA resonance (Fig. 4A and C) suggests induction of apoptosis in the tumor after MN58b treatment, which was confirmed by caspase-3 staining of tumor tissue sections. The increased saturated fatty acyl chain peak at 1.3 ppm may reflect the onset of necrosis in both treated and untreated tumors. Increased MR-visible lipids have been reported in stressed cells prior to cell death and suggests that the presence of lipid may reflect cellular responses to environmental or drug-induced stress (37, 40-44).

Our *in vivo* MRS findings (decreased tCho and tumor growth arrest) are consistent with the histological results in that MN58b-treated tumors had a reduction in the number of viable cells (Fig. 6). This indicates that MN58b not only inhibits ChoK activity but also leads to cell death and growth arrest, as is confirmed by the MTT assay *in vitro* and tumor size measurements by *in vivo* MRI. Despite significant growth arrest we did not observe a significant reduction of tumor volume with MN58b treatment, which may in part be due to a sub-optimal dose schedule of MN58b or route of administration (i.p. versus i.v. or oral gavage) of the drug during treatment. Caspase-3 staining did confirm an increase in apoptosis after MN58b treatment which was consistently associated with increased PUFA

resonances at 2.8 ppm (Fig. 4A and 6F, H). Similarly, a reduction in Hematoxylin stained cells was noted in MN58b-treated tumors indicating the efficacy of the drug (Fig. 6B, D). These findings suggest the potential role of MN58b as a complimentary therapeutic in the treatment of GBM patients.

Hypoxia is known to exist in brain tumors (45). Hypoxic tumor microenvironments pose a problem for radiation and chemotherapy; cancer cells located in hypoxic environments undergo adaptive responses, which render them resistant to radiation and chemotherapy, resulting in recurrence (46). Such resistance to treatment contributes to the incidence of cancer recurrence. Variations in the extent and degree of hypoxia/necrosis in combination with variable angiogenic patterns represent a considerable problem in radiotherapeutics and antiangiogenic management of GBM. Glunde *et al*. reported increased total choline and ChoK activity in a prostate cancer model and established a correlation between hypoxia, choline metabolites, and Chok activity. (46). These authors also suggested that hypoxia-inducible factor-1 (HIF-1) activation of hypoxia response elements within the putative ChoK promoter region can increase ChoK expression within hypoxic environments, consequently increasing cellular PC and tCho levels within these environments (46). It is known that GBMs are more heterogeneous and hypoxic compared to other types of brain tumors. Thus, it is plausible to hypothesize that inhibition of ChoK activity by a specific ChoK inhibitor may help in reducing the survival pathways which allow GBM tumors to thrive in hypoxic microenvironments, making them more sensitive for chemo and radiation therapy. However Bansal *et al.* have reported a decrease in choline phosphorylation in hypoxic prostate cancer cells which may result from other isoforms of hypoxia response elements (HRE) affecting ChoK activity in human brain tumors. There is intensifying urgency to find new drugs for the treatment of brain tumors (47). Development of anticancer agents is the key focus of several research studies on developing specific molecular targets against the malignant phenotype (5, 48, 49) with the ultimate goal of improving activity and therapeutic selectivity for tumor versus normal cells.

CONCLUSION

In conclusion, this study demonstrated that ^{1}H MRS can be used to detect a decrease in tCho that is associated with the inhibition of ChoK activity by MN58b in gliomas. These effects were seen in both cultured cells and in tumor xenografts. Significant reduction in tCho, elevated PUFA and increased apoptotic marker Caspase-3 after MN58b treatment demonstrates the potential of ChoK inhibition in GBM treatment. Monitoring metabolic changes with MRS may provide a noninvasive pharmacodynamic marker for ChoK inhibition and treatment-response in brain tumors.

ACKNOWLEDGEMENTS

MR data in this publication was obtained in the Small Animal Imaging Facility (SAIF) of the University of Pennsylvania. We thank Daniel Martinez of the Pathology Core Laboratory at the Children's Hospital of Philadelphia for performing histopathology of tumor tissue and assistance in histological quantification of the stained slides.

Financial support: Research reported in this publication was supported by the NIH R01-CA129176 (E.J. Delikatny), T32-GM8076 (S.P. Arlauckas), F31-CA180328 (S.P. Arlauckas) and DoD Breast Cancer Concept Award BC076631 (E.J. Delikatny).

List of Abbreviations

ChoK	choline kinase
CRLB	Cramer-Rao lower bound
D_2O	deuterium oxide
DMEM	Dulbecco's modified Eagle's medium
DMSO	dimethyl sulfoxide
GBM	Glioblastoma
GPC	glycerophosphocholine
H&E	Hematoxylin and Eosin
KOH	potassium hydroxide
MRS	magnetic resonance spectroscopy
MTT	3-(4,5-Dimethylthiazol-2-yl)-2,5-diphenyltetrazolium bromide
NMR	nuclear magnetic resonance
PBS	phosphate buffer saline
PC	phosphocholine
PCA	perchloric acid
tCho	total choline
TLC	thin layer chromatography
TSP	3-(trimethylsilyl) 3,3,3,3-tetradeuteropropionic acid
SPSS	statistical package for the social sciences
VAPOR	variable power and optimized relaxation delays

REFERENCES

1. Candolfi M, Curtin JF, Nichols WS, Muhammad AG, King GD, Pluhar GE, et al. Intracranial glioblastoma models in preclinical neuro-oncology: neuropathological characterization and tumor progression. J Neurooncol. 2007; 85:133–48. [PubMed: 17874037]
2. Gibbs JB. Mechanism-based target identification and drug discovery in cancer research. Science. 2000; 287:1969–73. [PubMed: 10720316]
3. Glunde K, Bhujwalla ZM, Ronen SM. Choline metabolism in malignant transformation. Nat Rev Cancer. 2011; 11:835–48. [PubMed: 22089420]
4. Aoyama C, Liao H, Ishidate K. Structure and function of choline kinase isoforms in mammalian cells. Prog Lipid Res. 2004; 43:266–81. [PubMed: 15003397]
5. Al-Saffar NM, Troy H, Ramirez de Molina A, Jackson LE, Madhu B, Griffiths JR, et al. Noninvasive magnetic resonance spectroscopic pharmacodynamic markers of the choline kinase inhibitor MN58b in human carcinoma models. Cancer Res. 2006; 66:427–34. [PubMed: 16397258]
6. Kennedy EP. Metabolism of lipides. Annu Rev Biochem. 1957; 26:119–48. [PubMed: 13488391]

7. Hernandez-Alcoceba R, Saniger L, Campos J, Nunez MC, Khaless F, Gallo MA, et al. Choline kinase inhibitors as a novel approach for antiproliferative drug design. Oncogene. 1997; 15:2289–301. [PubMed: 9393874]
8. Lacal JC. Choline kinase: a novel target for antitumor drugs. IDrugs. 2001; 4:419–26. [PubMed: 16015482]
9. Ramirez de Molina A, Rodriguez-Gonzalez A, Lacal JC. From Ras signalling to ChoK inhibitors: a further advance in anticancer drug design. Cancer Lett. 2004; 206:137–48. [PubMed: 15013519]
10. Ramirez de Molina A, Banez-Coronel M, Gutierrez R, Rodriguez-Gonzalez A, Olmeda D, Megias D, et al. Choline kinase activation is a critical requirement for the proliferation of primary human mammary epithelial cells and breast tumor progression. Cancer Res. 2004; 64:6732–9. [PubMed: 15374991]
11. Rodriguez-Gonzalez A, Ramirez de Molina A, Fernandez F, Ramos MA, del Carmen Nunez M, Campos J, et al. Inhibition of choline kinase as a specific cytotoxic strategy in oncogene-transformed cells. Oncogene. 2003; 22:8803–12. [PubMed: 14654777]
12. Rodriguez-Gonzalez A, Ramirez de Molina A, Fernandez F, Lacal JC. Choline kinase inhibition induces the increase in ceramides resulting in a highly specific and selective cytotoxic antitumoral strategy as a potential mechanism of action. Oncogene. 2004; 23:8247–59. [PubMed: 15378008]
13. Arlauckas SP, Popov AV, Delikatny EJ. Direct Inhibition of Choline Kinase by a Near-Infrared Fluorescent Carbocyanine. Mol Cancer Ther. 2014; 13:1–10.
14. Kapoor GS, Poptani H, Hsu O, Kim S, O'Rourke D. In vivo analysis of EGFRvIII rat glioma growth and invasion by magnetic resonance imaging (MRI). Neuro-Oncol. 2007; 9:467–602.
15. Covington AK, Paabo M, Robinson RA, Bates RG. Use of the glass electrode in deuterium oxide and the relation between the standardized pD (paD) scale and the operational pH in heavy water. Anal Chem. 1968; 40:700–6.
16. Huszthy PC, Daphu I, Niclou SP, Stieber D, Nigro JM, Sakariassen PO, et al. In vivo models of primary brain tumors: pitfalls and perspectives. Neuro Oncol. 2012; 14:979–93. [PubMed: 22679124]
17. Bryant MJ, Chuah TL, Luff J, Lavin MF, Walker DG. A novel rat model for glioblastoma multiforme using a bioluminescent F98 cell line. J Clin Neurosci. 2008; 15:545–51. [PubMed: 18378459]
18. Tkac I, Starcuk Z, Choi IY, Gruetter R. In vivo 1H NMR spectroscopy of rat brain at 1 ms echo time. Magn Reson Med. 1999; 41:649–56. [PubMed: 10332839]
19. Kyrylkova K, Kyryachenko S, Leid M, Kioussi C. Detection of apoptosis by TUNEL assay. Methods Mol Biol. 2012; 887:41–7. [PubMed: 22566045]
20. Evanochko WT, Ng TC, Glickson JD. Application of in vivo NMR spectroscopy to cancer. Magn Reson Med. 1984; 1:508–34. [PubMed: 6400586]
21. Provencher SW. Automatic quantitation of localized in vivo 1H spectra with LCModel. NMR Biomed. 2001; 14:260–4. [PubMed: 11410943]
22. Ruifrok AC, Johnston DA. Quantification of histochemical staining by color deconvolution. Anal Quant Cytol Histol. 2001; 23:291–9. [PubMed: 11531144]
23. Aboagye EO, Bhujwalla ZM. Malignant transformation alters membrane choline phospholipid metabolism of human mammary epithelial cells. Cancer Res. 1999; 59:80–4. [PubMed: 9892190]
24. Ramirez de Molina A, Sarmentero-Estrada J, Belda-Iniesta C, Taron M, Ramirez de Molina V, Cejas P, et al. Expression of choline kinase alpha to predict outcome in patients with early-stage non-small-cell lung cancer: a retrospective study. Lancet Oncol. 2007; 8:889–97. [PubMed: 17851129]
25. Ramirez de Molina A, Gutierrez R, Ramos MA, Silva JM, Silva J, Bonilla F, et al. Increased choline kinase activity in human breast carcinomas: clinical evidence for a potential novel antitumor strategy. Oncogene. 2002; 21:4317–22. [PubMed: 12082619]
26. McCann CM, Waterman P, Figueiredo JL, Aikawa E, Weissleder R, Chen JW. Combined magnetic resonance and fluorescence imaging of the living mouse brain reveals glioma response to chemotherapy. Neuroimage. 2009; 45:360–9. [PubMed: 19154791]
27. Foster DA, Xu L. Phospholipase D in cell proliferation and cancer. Mol Cancer Res. 2003; 1:789–800. [PubMed: 14517341]

28. Sanchez-Lopez E, Zimmerman T, Gomez del Pulgar T, Moyer MP, Lacal Sanjuan JC, Cebrian A. Choline kinase inhibition induces exacerbated endoplasmic reticulum stress and triggers apoptosis via CHOP in cancer cells. Cell Death Dis. 2013; 4:e933. [PubMed: 24287694]
29. Doblas S, He T, Saunders D, Hoyle J, Smith N, Pye Q, et al. In vivo characterization of several rodent glioma models by 1H MRS. NMR Biomed. 2012; 25:685–94. [PubMed: 21954105]
30. Young GS. Advanced MRI of adult brain tumors. Neurol Clin. 2007; 25:947–73. viii. [PubMed: 17964022]
31. Podo F. Tumour phospholipid metabolism. NMR Biomed. 1999; 12:413–39. [PubMed: 10654290]
32. Ronen SM, Jackson LE, Beloueche M, Leach MO. Magnetic resonance detects changes in phosphocholine associated with Ras activation and inhibition in NIH 3T3 cells. Br J Cancer. 2001; 84:691–6. [PubMed: 11237392]
33. Opstad KS, Bell BA, Griffiths JR, Howe FA. An investigation of human brain tumour lipids by high-resolution magic angle spinning 1H MRS and histological analysis. NMR Biomed. 2008; 21:677–85. [PubMed: 18186027]
34. Kuesel AC, Briere KM, Halliday WC, Sutherland GR, Donnelly SM, Smith IC. Mobile lipid accumulation in necrotic tissue of high grade astrocytomas. Anticancer Res. 1996; 16:1485–9. [PubMed: 8694517]
35. Kuesel AC, Sutherland GR, Halliday W, Smith IC. 1H MRS of high grade astrocytomas: mobile lipid accumulation in necrotic tissue. NMR Biomed. 1994; 7:149–55. [PubMed: 8080717]
36. Griffin JL, Lehtimaki KK, Valonen PK, Grohn OH, Kettunen MI, Yla-Herttuala S, et al. Assignment of 1H nuclear magnetic resonance visible polyunsaturated fatty acids in BT4C gliomas undergoing ganciclovir-thymidine kinase gene therapy-induced programmed cell death. Cancer Res. 2003; 63:3195–201. [PubMed: 12810648]
37. Hakumaki JM, Poptani H, Sandmair AM, Yla-Herttuala S, Kauppinen RA. 1H MRS detects polyunsaturated fatty acid accumulation during gene therapy of glioma: implications for the in vivo detection of apoptosis. Nat Med. 1999; 5:1323–7. [PubMed: 10546002]
38. Lee SC, Delikatny EJ, Poptani H, Pickup S, Glickson JD. In vivo (1)H MRS of WSU-DLCL2 human non-Hodgkin's lymphoma xenografts: response to rituximab and rituximab plus CHOP. NMR Biomed. 2009; 22:259–65. [PubMed: 19040203]
39. Lee SC, Poptani H, Pickup S, Jenkins WT, Kim S, Koch CJ, et al. Early detection of radiation therapy response in non-Hodgkin's lymphoma xenografts by in vivo 1H magnetic resonance spectroscopy and imaging. NMR Biomed. 2010; 23:624–32. [PubMed: 20661875]
40. Liimatainen T, Lehtimaki K, Ala-Korpela M, Hakumaki J. Identification of mobile cholesterol compounds in experimental gliomas by (1)H MRS in vivo: effects of ganciclovir-induced apoptosis on lipids. FEBS Lett. 2006; 580:4746–50. [PubMed: 16893542]
41. Delikatny E, Jeitner T. The accumulation of H-1 MR-visible lipid in human glioma cells is independent of the cell cycle. Int J Oncol. 1997; 11:543–50. [PubMed: 21528245]
42. Delikatny EJ, Chawla S, Leung DJ, Poptani H. MR-visible lipids and the tumor microenvironment. NMR Biomed. 2011; 24:592–611. [PubMed: 21538631]
43. Milkevitch M, Shim H, Pilatus U, Pickup S, Wehrle JP, Samid D, et al. Increases in NMR-visible lipid and glycerophosphocholine during phenylbutyrate-induced apoptosis in human prostate cancer cells. Biochim Biophys Acta. 2005; 1734:1–12. [PubMed: 15866478]
44. Roman SK, Jeitner TM, Hancock R, Cooper WA, Rideout DC, Delikatny EJ. Induction of magnetic resonance-visible lipid in a transformed human breast cell line by tetraphenylphosphonium chloride. Int J Cancer. 1997; 73:570–9. [PubMed: 9389574]
45. Vartanian A, Singh SK, Agnihotri S, Jalali S, Burrell K, Aldape KD, et al. GBM's multifaceted landscape: highlighting regional and microenvironmental heterogeneity. Neuro Oncol. 2014; 16:1167–75. [PubMed: 24642524]
46. Glunde K, Shah T, Winnard PT Jr. Raman V, Takagi T, Vesuna F, et al. Hypoxia regulates choline kinase expression through hypoxia-inducible factor-1 alpha signaling in a human prostate cancer model. Cancer Res. 2008; 68:172–80. [PubMed: 18172309]
47. Bansal A, Harris RA, DeGrado TR. Choline phosphorylation and regulation of transcription of choline kinase alpha in hypoxia. J Lipid Res. 2012; 53:149–57. [PubMed: 22025560]

48. Workman P, Kaye SB. Translating basic cancer research into new cancer therapeutics. Trends Mol Med. 2002; 8:S1–9. [PubMed: 11927279]

49. Gelmon KA, Eisenhauer EA, Harris AL, Ratain MJ, Workman P. Anticancer agents targeting signaling molecules and cancer cell environment: challenges for drug development? J Natl Cancer Inst. 1999; 91:1281–7. [PubMed: 10433616]

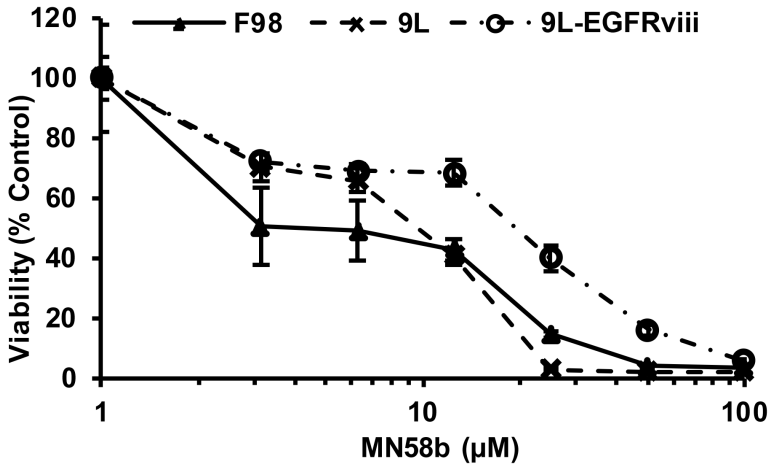

Figure 1.

MTT assay demonstrating inhibition of cellular viability of F98, 9L and 9L-EGFRviii cell lines with MN58b. 24 h MN58b exposure significantly reduced the viability of the F98, 9L and 9L-EGFRviii cells in a dose dependent manner. The data was normalized to untreated control cells and represents the average ± SEM of 3 separate experiments performed in quadruplicate.

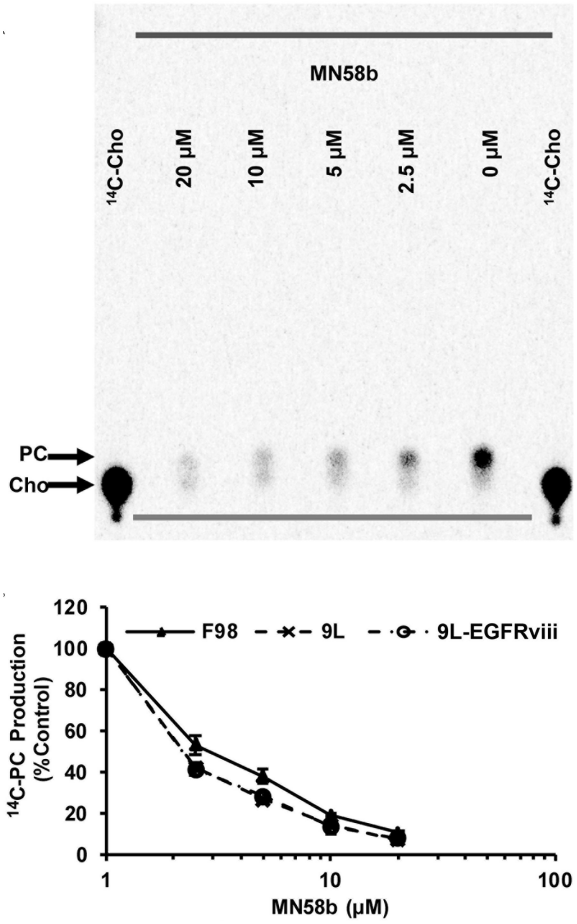

Figure 2.

Effect of MN58b on ChoK activity in tumor cells. Autoradiography of TLC-separated ^{14}C-choline containing metabolites (A) allows for the quantification of ^{14}C-PC and demonstrates a dose-dependent reduction of choline phosphorylation in response to MN58b treatment. The graph (B) shows a dose dependent reduction of ChoK activity in the F98, 9L and 9L-EGFRviii cell lines. Error bars represent ± SEM of 3 separate experiments.

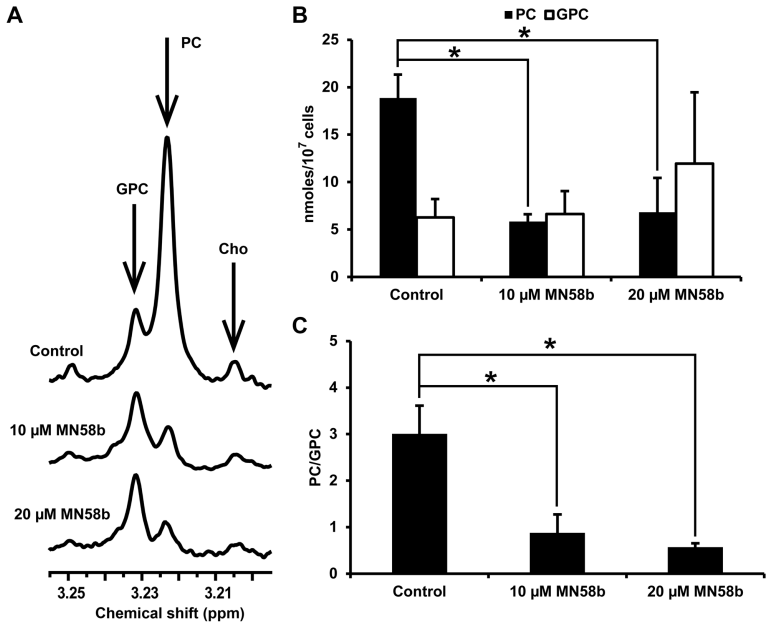

Figure 3.

In vitro NMR of F98 cell extracts (A). Untreated cells display high levels of PC (3.22 ppm) and low levels of GPC (3.23 ppm) (top spectrum); 10 μM MN58b reduces the PC resonance relative to GPC (middle spectrum) and 20 μM MN58b further reduces this ratio (bottom spectrum). (B) A bar graph showing the quantitation of PC and GPC from untreated, 10 and 20 μM MN58b-treated cells (C). The PC/GPC ratio demonstrates differences between untreated, 10 and 20 μM MN58b-treated cells. Asterisk (*) represents significant differences with a p-value of <0.05. Error bars represent ± SEM of 3 separate experiments.

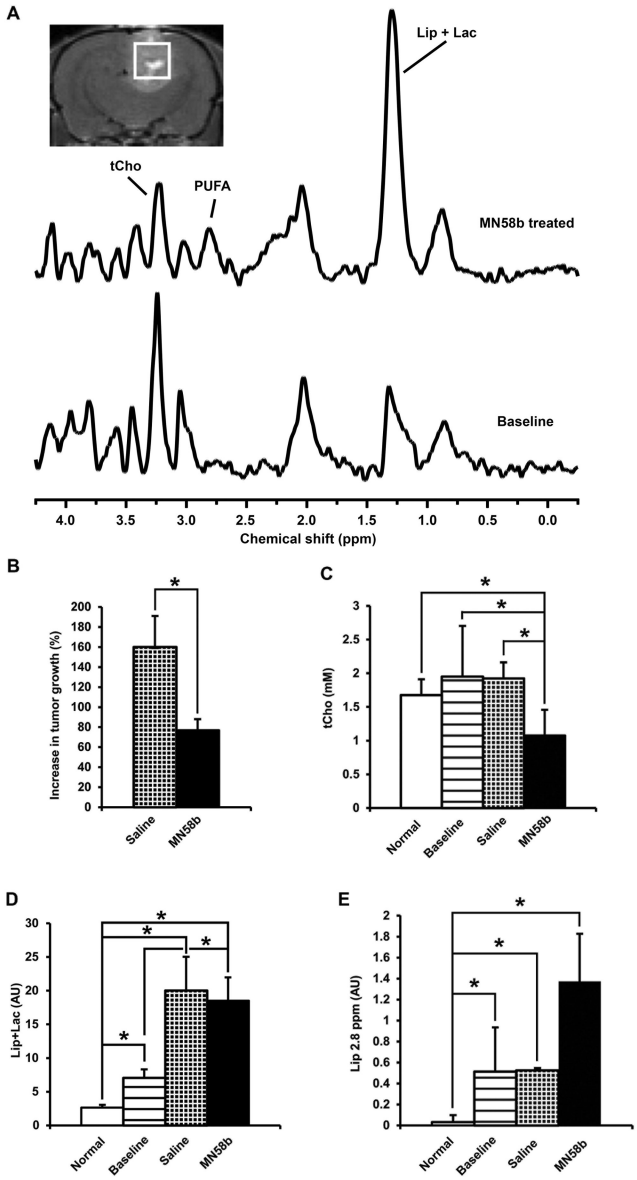

Figure 4.

Representative *in-vivo* ^{1}H MR Spectrum (A) from baseline untreated F98 tumor (bottom line) and MN58b treated (top line) tumor. The MR image demonstrates placement of the voxel for *in vivo* MRS studies. Bar graph (B) demonstrates the percentage changes in volume in saline-treated (checked) and MN58b-treated (black) tumors. Normal tissue is represented by the white bar. The baseline untreated tumor demonstrates high tCho (horizontal lines, C) and low Lip/lac (D). MN58b treatment (black) resulted in reduced tCho and increased Lip/lac level at 1.3 ppm (D) and polyunsaturated lipids at 2.8 ppm (Lip2.8) (E). Asterisk (*) represents significant differences with a p-value of <0.05. Error bars represent ± SEM.

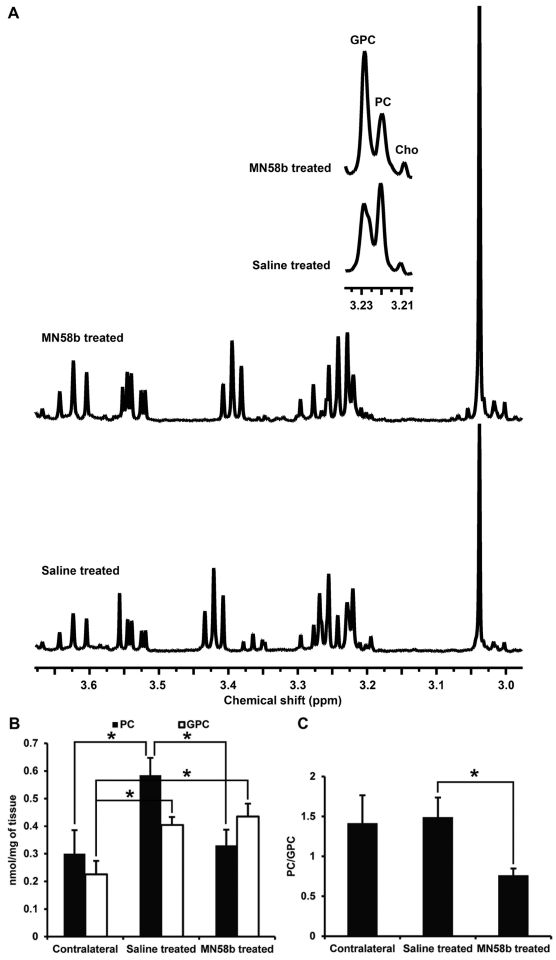

Figure 5.

(A) Representative *in vitro* ^{1}H NMR spectrum from perchloric acid extracts of saline-treated (bottom) and MN58b-treated F98 tumors (top). The zoomed region (inset) is the spectral region from the choline-containing metabolites. Bar graph (B) demonstrates changes in PC and GPC levels from contralateral normal tissue, saline-treated tumors and MN58b-treated tumors. Bar graph (C) demonstrates the PC/GPC ratio in the 3 groups. Asterisk (*) represents significant differences with a p-value of <0.05. Error bars represent ± SEM.

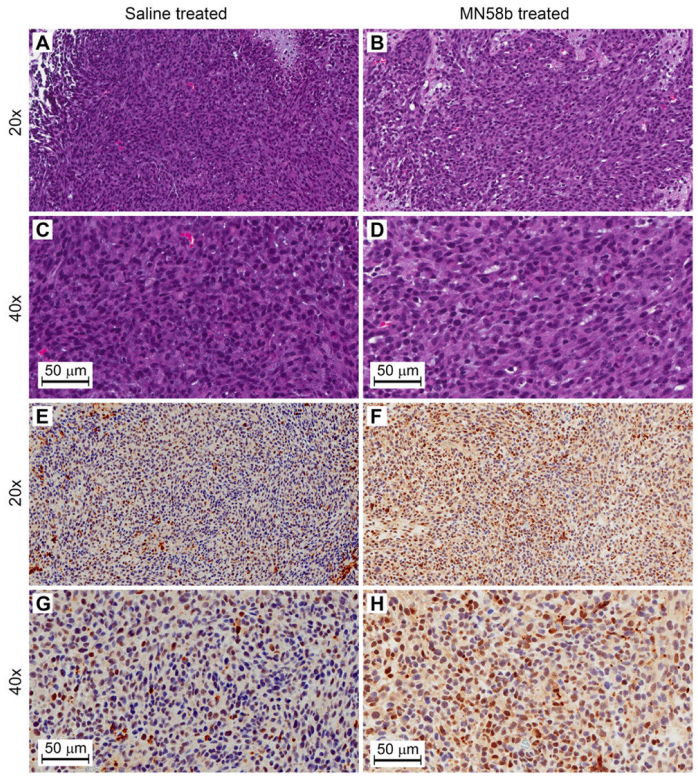

Figure 6.

Representative histological sections from saline-treated and MN58b-treated F98 rat brain tumors. H&E (A to D, 20 and 40x) and Caspase-3 (E to H, 20 and 40x) immunohistochemistry in tumor sections demonstrating decreased cell density in MN58b-treated tumors (B and D) compared to saline-treated tumors (A and C). Caspase-3 positive cells are increased in MN58b-treated tumors (F and H) compared to saline-treated tumors (E and G) indicating increased apoptosis. Scale bar is 50 μm.